Simulated Atmospheric Response to Four Projected Land-Use Land-Cover Change Scenarios for 2050 in the North-Central United States

PAUL XAVIER FLANAGAN,[a] REZAUL MAHMOOD,[b,c] TERRY SOHL,[d] MARK SVOBODA,[c,e] BRIAN WARDLOW,[c,f] MICHAEL HAYES,[c] AND ERIC RAPPIN[g]

[a] *U.S. Department of Agriculture Agricultural Research Service, El Reno, Oklahoma*
[b] *High Plains Regional Climate Center, University of Nebraska–Lincoln, Lincoln, Nebraska*
[c] *School of Natural Resources, University of Nebraska–Lincoln, Lincoln, Nebraska*
[d] *U.S. Geological Survey Earth Resources Observation and Science Center, Sioux Falls, South Dakota*
[e] *National Drought Mitigation Center, University of Nebraska–Lincoln, Lincoln, Nebraska*
[f] *Center for Advanced Land Management Information Technologies, University of Nebraska–Lincoln, Lincoln, Nebraska*
[g] *Kentucky Climate Center, Western Kentucky University, Bowling Green, Kentucky*

(Manuscript received 29 September 2020, in final form 20 August 2021)

ABSTRACT: Land-use land-cover change (LULCC) has become an important topic of research for the central United States because of the extensive conversion of the natural prairie into agricultural land, especially in the northern Great Plains. As a result, shifts in the natural climate (minimum/maximum temperature, precipitation, etc.) across the north-central United States have been observed, as noted within the Fourth National Climate Assessment (NCA4) report. Thus, it is necessary to understand how further LULCC will affect the near-surface atmosphere, the lower troposphere, and the planetary boundary layer (PBL) atmosphere over this region. The goal of this work was to investigate the utility of a new future land-use land-cover (LULC) dataset within the Weather Research and Forecasting (WRF) modeling system. The present study utilizes a modeled future land-use dataset developed by the Forecasting Scenarios of Land-Use Change (FORE-SCE) model to investigate the influence of future (2050) land use on a simulated PBL development within the WRF Model. Three primary areas of LULCC were identified within the FORE-SCE future LULC dataset across Nebraska and South Dakota. Variations in LULC between the 2005 LULC control simulation and four FORE-SCE simulations affected near-surface temperature (0.5°–1°C) and specific humidity (0.3–0.5 g kg^{-1}). The differences noted in the temperature and moisture fields affected the development of the simulated PBL, leading to variations in PBL height and convective available potential energy. Overall, utilizing the FORE-SCE dataset within WRF produced notable differences relative to the control simulation over areas of LULCC represented in the FORE-SCE dataset.

KEYWORDS: North America; Convective-scale processes; Atmosphere–land interaction; Numerical analysis/modeling; Regional models

1. Introduction

Land-use land-cover (LULC) plays an important role in regional and global climate systems (Bonan et al. 2004; Torbick et al. 2006; Wang et al. 2006; Pyke and Andelman 2007; Mahmood et al. 2014, 2016; Pielke et al. 2016; Sleeter et al. 2018). As stated in the Fourth National Climate Assessment (NCA4), "changes in land-cover continue to impact local- to global-scale weather and climate by altering the flow of energy, water, and greenhouse gases between the land and the atmosphere (high confidence)" (Sleeter et al. 2018, p. 212). This primarily reflects the effects of LULC on radiation, through changes in albedo, surface radiation balance, and differences in moisture content (Pielke 2005; Pielke et al. 2011; Pitman et al. 2011; Fahey et al. 2017). LULC influences the surface radiative balance via changes to partitioning of energy into sensible and latent heat fluxes during the daytime (e.g., Harding and Snyder 2012a,b; Aegerter et al. 2017; Chen et al. 2017; Chen and Dirmeyer 2017). Hence, LULC change (LULCC) further modifies near-surface air temperatures and moisture content.

Koster et al. (2004) have shown that the central United States is strongly affected by land–atmosphere interactions. As LULC is intrinsically linked to soil moisture, the process of coupling between soil moisture and precipitation occurs through various processes linked to different LULC types. For example, the transition from natural grasslands to irrigated agriculture during the twentieth century has notably changed the temperature and moisture regime in the region, namely, cooler daytime surface temperatures, warmer minimum temperatures, and increases of near-surface moisture (Mahmood et al. 2004). Mahmood et al. (2006, 2013) subsequently found that increases in the coverage of irrigated cropland decreased mean maximum growing season temperatures by >1°C after 1945. Mahmood et al. (2006) also noted >1°C increase in growing season minimum temperatures in the post-1945 period. In another study, Mahmood et al. (2004) found a downward trend in mean and mean maximum growing season temperatures across areas that had increases in irrigated lands from 1921 to 2000. Although LULCC lowered the maximum temperature in certain regions such as those with intensive agricultural irrigation, the increasing temperature signal was strengthened in other regions, for example changing

Corresponding author: Paul Flanagan, paul.flanagan2@usda.gov

Earth Interactions is published jointly by the American Meteorological Society, the American Geophysical Union, and the Association of American Geographers.

DOI: 10.1175/EI-D-20-0019.1

from natural vegetation to pasture in the Brazilian Cerrado (Pielke et al. 2011). In terms of variability, LULCC has been linked to changes in the frequency of midlatitude hot and dry summers globally (Findell et al. 2017), particularly in areas with conversion of forest to croplands.

LULC influences diurnal development of the planetary boundary layer (PBL). Differences in PBL evolution can influence convective potentials (Findell and Eltahir 2003a,b; Koster et al. 2004; Jimenez et al. 2014), which cause further surface moisture discontinuities and modify subsequent convective environments. Thus, LULCC can further affect PBL evolution and convective potentials and influence synoptic and mesoscale weather patterns (Segal and Arritt 1992; Garcia-Carreras et al. 2010; Nair et al. 2011; Huber et al. 2014). As the effects of LULCC are felt on the meteorological scale, they also affect broader global climate. For example, thunderstorms occur over a relatively smaller percentage of Earth's surface, however, they redistribute a vast amount of energy and have synoptic-scale effects (Pielke 2005). In other words, as changes are made to Earth's surface on a relatively smaller scales, the resulting modifications can affect regional and or global-scale climate.

Past studies have shown the importance of including LULC in global circulation models to produce more accurate representations of global and regional climate systems (Zhao et al. 2001; Zhao and Pitman 2002; Costa et al. 2007; Ge et al. 2007; Spera et al. 2018). Ge et al. (2007) found that accuracy of precipitation estimates by regional climate models were reduced when LULC data of less than 80% accuracy were used. Spera et al. (2018) showed that accurate, regionally validated land-cover data improve model simulation results. They demonstrated that by incorporating the improved land-cover dataset, model performance with regard to precipitation had increased especially in the dry-to-wet season transition. Again, it is evident that accurate representations of land cover within model simulations are crucial to properly represent surface processes on both meteorological and climatological scales.

LULCC is expected to continue in the coming decades because of increased demands for food, energy, and urban development (Veldkamp and Lambin 2001; Sohl et al. 2014). Several studies (e.g., Wear 2011; Bierwagen et al. 2010; Lawler et al. 2014; Sohl et al. 2014, 2016) have developed simulated future LULCC datasets for potential future socioeconomic conditions. This study uses four such newly developed datasets to address its research goals, that is, to determine the effects of using the Forecasting Scenarios of Land-Use Change (FORE-SCE) LULC dataset within the Weather, Research, and Forecasting (WRF) Model system.

The objective of this research is to determine the effects of four 2050 LULCC scenarios on a simulated near-surface atmosphere, lower troposphere, and the PBL under synoptically calm conditions in the north-central United States (NCUS), or the states of Nebraska and South Dakota (Fig. 1a). These applications also allowed us to better understand the utility of FORE-SCE LULC in the WRF modeling suite for short-term coupled weather simulations. The LULCC scenarios were developed by using the U.S. Geological Survey (USGS) FORE-SCE LULC modeling system (Sohl et al. 2007, 2012, 2014). To complete this project, the Advanced Research version of WRF (ARW) modeling system (Skamarock et al. 2019) along with the FORE-SCE model's four future LULCC projected datasets were used.

The design of this study is such that it also allowed the effects of the FORE-SCE dataset to be determined in WRF-based simulations. This is achieved by comparing and analyzing the LULC fields within the FORE-SCE LULC historical data (Fig. 1b) and WRF default LULC data [Moderate Resolution Imaging Spectroradiometer (MODIS) LULC; Fig. 1c]. These results can aid in developing future FORE-SCE and WRF related research, especially for potential effects of different FORE-SCE scenarios within climate length WRF simulations. Subsequently, WRF-based atmospheric simulations for all four 2050 FORE-SCE scenarios, along with a control simulation using FORE-SCE 2005 historical data, were completed.

To the best of our knowledge this is one of the first adoptions of these datasets for regional-scale model applications focusing on the effects of atmospheric evolution within the boundary layer. While Nikolic et al. (2019) utilized the FORE-SCE dataset within WRF, their study focused on the effects of LULCC on the central U.S. low-level jet and its development within a climate time-scale simulation. In the sections 2 and 3, the methods applied and the results of the research, respectively, are presented. A discussion and conclusions of this study in the context of previous results relating to NCUS LULCC are provided in sections 4 and 5, respectively.

2. Methods

a. FORE-SCE future LULC dataset

The FORE-SCE LULC dataset is produced using a patch-based model broken into 84 Level III ecoregions of the United States as mapped for the 1999 U.S. Environmental Protection Agency (EPA) ecoregion publication (EPA 1999). The model uses a nonspatial "demand" component to produce the future proportions of LULCC at a regional level (Sohl et al. 2014). Demand for a "historical" period of 1992–2005 was based on LULC proportions from the USGS land-cover trends data (Loveland et al. 2002). The historical baseline dataset was created by remapping the 1992 National Land Cover Database (NLCD; Vogelmann et al. 2001) to the FORE-SCE dataset thematic classes at a 250-m gridcell resolution. Then the FORE-SCE model was driven by the 1992–2005 NLCD dataset and USGS land-cover trends to create the 1992–2005 FORE-SCE historical baseline data. Future scenarios for the 2006–2100 period are based on the IPCC Special Report on Emissions Scenarios (SRES; Nakićenović et al. 2000), downscaled to the regional level for use within the FORE-SCE model. The scenario-based FORE-SCE projections were designed to provide a high-resolution and thematically detailed future LULC dataset for investigating the effects of LULCC on ecology, carbon and greenhouse gas fluxes, climate and weather, and hydrology (Sohl et al. 2014).

The LULCC data are available from the USGS data repository (https://doi.org/10.5066/P95AK9HP; Sohl et al. 2018) at a 250-m spatial resolution. The FORE-SCE LULCC dataset has 17 LULC categories (Table 1) that are similar to the NLCD LULC categories (Homer et al. 2007), with data

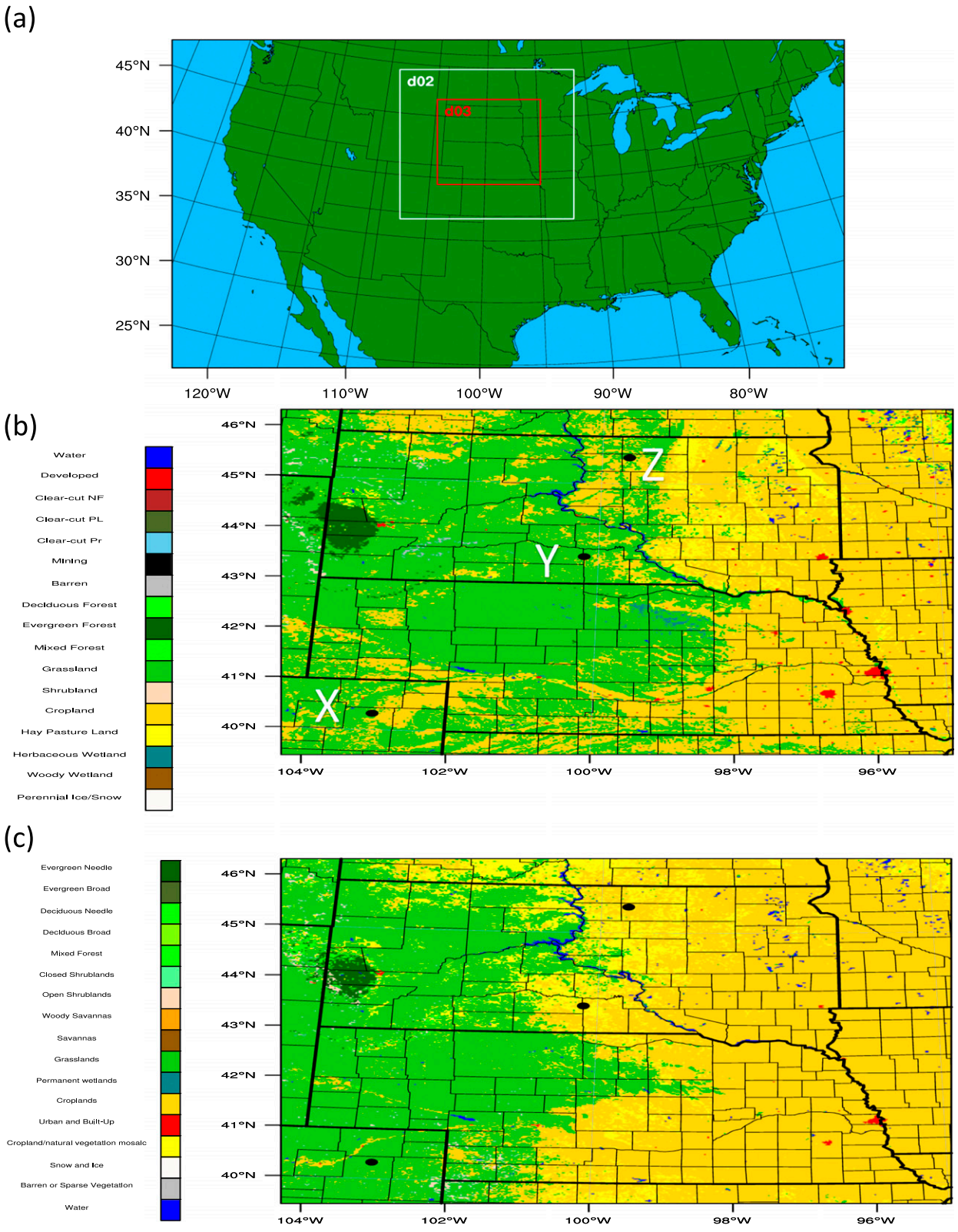

FIG. 1. (a) The WRF domain used within the study. The red outline shows the inner domain used to create the spatial plots for this study. (b) The FORE-SCE 2005 Historical LULC dominant category within the inner WRF domain used in the study. (c) The WRF default MODIS LULC dominant category within the inner WRF domain. Also shown in (b) and (c) are dots denoting the location of the three vertical profile locations; location X (northeastern Colorado), location Y (central Nebraska–South Dakota border), and location Z (north-central South Dakota).

TABLE 1. List of land-use categories within the FORE-SCE LULC dataset.

1	Water
2	Developed
3	Mechanically disturbed national forests
4	Mechanically disturbed other public lands
5	Mechanically disturbed private
6	Mining
7	Barren
8	Deciduous forest
9	Evergreen forest
10	Mixed forest
11	Grassland
12	Shrubland
13	Cropland
14	Hay/pasture land
15	Herbaceous wetland
16	Woody wetland
17	Perennial ice/snow

available from 2006 to 2100 for the conterminous United States for four different IPCC scenarios. These scenarios include the A1B (rapid economic growth with balanced energy use across all technologies), A2 (continuous population growth), B1 (rapid economic changes to more service and technology with global environmental protection) and B2 (local/regional environmental protection), with further descriptions included in Table 2.

The data are available in GeoTIFF format and were processed into a format (geogrid binary format) usable by the WRF Pre-Processing System (WPS) using the QGIS processing system and the GIS4WRF package. The FORE-SCE LULC data were then included in the WRF simulations through incorporation of the dataset into the WPS prior to the production of the wrfinput files. We utilized 2050 datasets instead of the 2100 datasets because the 2050 datasets provide a more realistic representation of future LULC owing to the source IPCC SRES scenarios, as the simulated differences in the LULCC data become more exaggerated in longer historical LULC projections (Sohl et al. 2014). The WRF simulation output data were processed and plotted using internal code within the NCAR Command Language (NCL) available from NCAR (https://www.ncl.ucar.edu/).

b. *WRF Model configuration*

The WRF Model, version 4.0.3 (Skamarock et al. 2019), was used to simulate the evolution of the PBL under inactive atmospheric conditions for 1200 UTC 1 August–1200 UTC 8 August 2001, with the first three days constituting model spinup/dynamic adjustment time. While 3 days likely does not constitute enough spinup time for soil moisture levels to equilibrate with the new LULC data, the stated goal is to determine the influence of the new LULC on the atmosphere. If soil moisture values are modified based on the LULCC, the effects of the modified soil moisture values would also facilitate differences in atmospheric fields causing additional differences that could not be untangled from the LULCC forced differences. In other words, the soil moisture state could still reflect the input data's land surface parameters rather than adjusting to the new LULC dataset. Thus, our results could be affected by model-specific soil moisture, which cannot be disentangled from the effects caused by the LULCC. As this study serves as a proof-of-concept work on the use of the FORE-SCE dataset within WRF, a robust evaluation of the effect of LULCC versus soil moisture on the atmosphere is not warranted.

The WRF is a mesoscale and nonhydrostatic atmospheric model, which can be configured either for research or operational use. For this study, a nested domain containing two outer domains and the inner (analysis) domain was used (Fig. 1a). The outer domains were at 30- and 10-km resolutions, with the inner domain at a 2-km horizontal resolution with 38 vertical levels. The primary analysis was done on the 401×386 gridpoint inner domain centered on South Dakota and Nebraska. The final configuration (Table 3) was determined through sensitivity testing and comparing configurations of previous modeling studies completed over the same region (e.g., Harding and Snyder 2012a,b; Pei et al. 2016; Aegerter et al. 2017). Noah-MP (Niu et al. 2011) was used to get a baseline of the influence of the Noah-MP land surface model utilized with the FORE-SCE dataset. The North American Regional Reanalysis (NARR; Mesinger et al. 2006) dataset was used for initial and boundary conditions for all simulations.

The default LULC dataset used for these WRF simulations was the 17-class FORE-SCE 2005 historical land-cover data (Sohl et al. 2014). This dataset contains the same land-cover types used by FORE-SCE and is the final year in the 1992–2005 FORE-SCE historical baseline period. The FORE-SCE 2005 historical data were compared with the WRF default 20-class MODIS land-cover dataset. This dataset contains 17 land-cover types classified by the International Geosphere–Biosphere Programme (Friedl et al. 2002) and three tundra classes (Justice et al. 2002). The MODIS LULC dataset was compiled using MODIS data from 2001 to 2010 (Broxton et al. 2014) and was designed to work with the Noah LSM within WRF (Li et al. 2014).

To utilize the FORE-SCE data within WRF, substantial changes to several variable tables related to the land surface were needed, namely to the LANDUSE.TBL, VEGPARM.TBL, and MPTABLE.TBL tables. The new LULC dataset would normally require tuning of variables for the new LULC categories. However, because of the FORE-SCE LULC categories were based on the NLCD LULC categories (Sohl et al. 2014), it was possible to use the WRF table variable parameters for other LULC categories. Parameters within relevant variable tables were taken from the same or similar LULC categories in different LULC datasets. If the LULC categories within FORE-SCE datasets were not available in the NLCD dataset, details from Sohl et al. (2014) were used to derive the best possible variable parameters. For example, the urban class within FORE-SCE datasets is an aggregate category composed of the NLCD dataset's low-intensity residential, high-intensity residential, commercial/industrial/transportation, and urban/recreation grass classes (Sohl et al. 2014).

c. *Data analysis*

Differences were calculated by subtracting the control simulation from the FORE-SCE WRF simulations (FORE-SCE minus control). Thus, positive and negative differences

TABLE 2. Description of IPCC SRES scenarios used within the Sohl et al. (2014) study to develop the FORE-SCE LULC datasets used within this study. Descriptions are summarized from Nakićenović et al. (2000).

Scenario	Description of main drivers
A2	Economic growth is focused into specific economic regions
	Highlighted by lower trade flows and slower technological change
	Less international cooperation relative to other scenarios
	Advances in technology diffuse across regions slowly
	Large population growth through 2100
	Per capita income is lower than other scenarios
	Local resources prioritized, import dependence minimized through technological advances
	Global environmental concerns are weak; focus is on local and regional protections as necessary to control pollution
A1B	Economically driven scenario; average income per capita converge across the globe
	Technological advances prioritized, play central role in economic growth
	Population growth to 2050 and then decline to 2100
	Prioritizes a mixture/balance of supply and technological resources
	Advances in technology and supply are such that no one energy resource becomes overly dominant
B1	Environmental and social conscious development
	Focused on globally coherent approach to more sustainable development
	Governments, businesses, the media, and the public pay increased attention to the environmental and social aspects of development
	Scenario is not driven by climate policies
	Population increases to 2050 and then decreases to 2100
	Technological advances are prioritized in resource use efficiency rather than in productivity as in the A1 scenarios
B2	More balanced scenarios relative to the others
	Local and regional decision-making structures are prioritized over international institutions
	Humane welfare, equality, and environmental protections are all prioritized
	Population growth continuous until 2100
	Slower rate of technological and economic development
	Technological and economic advancement are regionally heterogeneous
	Global priorities largely do not exist in this scenario
	Environmental protection strategies are not as successful on a large scale relative to other scenarios
	High levels of education and social innovation

indicate higher and lower meteorological values, respectively, under FORE-SCE LULCC scenarios. To diagnose the influence of the LULCC on the simulated PBL development, composites were created by averaging across all hours within each daytime and nighttime period, for both the daytime (1200–0000 UTC) and nighttime (0000–1200 UTC) for 1200 UTC 4 August–1200 UTC 8 August 2001, with 1200 UTC 1 August–1100 UTC 4 August constituting model spin up/dynamic adjustment time. The variables investigated were 2-m temperature, vertical temperature (°C) from the surface through the top of the troposphere, surface heat fluxes (latent and sensible heat; W m^{-2}), 2-m specific humidity (g kg^{-1}), PBL height (PBLH) (m), and vertical dewpoint temperature (°C) from the surface through the top of the troposphere.

TABLE 3. Configuration of WRF used within this study.

Horizontal resolution	30/10/2 km
Vertical resolution	38 levels
Time step	30 s
Boundary conditions	NARR
LSM	Noah-MP
Dynamic vegetation	Noah-MP
Longwave radiation	Rapid Radiative Transfer Model
Shortwave radiation	Dudhia scheme
Microphysics	WRF single-moment 6-class
PBL	Yonsei University scheme
Cumulus parameterization	Kain–Fritsch scheme (only for 30- and 10-km domains)
Static surface data	Default

Vertical difference profiles were created for three locations shown as X, Y, and Z in Fig. 1b. The three locations were chosen due to shifts in LULC found across the four FORE-SCE scenarios. In comparison with the 2005 FORE-SCE historical dataset, the 2050 FORE-SCE scenarios show a variety of differing LULCC at the three locations analyzed for this study. In the 2050 FORE-SCE scenarios, location X (northeastern Colorado) shows LULCC from cropland to grassland in scenario B2 while the three other scenarios show small increases of cropland from grassland; location Y (central Nebraska–South Dakota border) depicts LULCC from grassland to hay/pasture or cropland; and location Z (north-central South Dakota) shows LULCC from grassland to cropland.

3. Results

a. *Projected LULCC*

As MODIS LULC is the default WRF LULC dataset, it would be useful to compare the FORE-SCE 2005 historical baseline LULC data with the MODIS LULC dataset. The

MODIS LULC dataset (20 categories) has more thematic classification categories than does FORE-SCE (17 categories). Further, MODIS represents a LULC climatology from 2001 to 2010 (Broxton et al. 2014), with the 2005 historical FORE-SCE data chosen owing to it being the final year in the historical FORE-SCE simulation. The largest difference in categories between the two LULC datasets within the study domain is the cropland/nature vegetation mosaic category in MODIS. This mosaic category is not replicated within the FORE-SCE dataset while the hay/pasture category shows the most commonality with the WRF parameter tables. This is a result of spatial resolution, as the 30-m-resolution FORE-SCE data did not require split land-cover types, which was necessary in the 500-m-resolution MODIS data.

After interpolating the LULC data to the WRF grid by utilizing the WPS, a direct comparison of the two LULC datasets can be completed. There are three primary categories that change between the two datasets: 1) grassland, 2) cropland, and 3) the hay/pasture or natural/cropland mosaic categories. The FORE-SCE 2005 data (Fig. 1b) extends the grassland area much farther to the east relative to the MODIS data (Fig. 1c). The increase in grassland (27% increase) area comes at the expense of the cropland (9% decrease) and natural/cropland mosaic (51% decrease) area. Relative to MODIS, the latter also decreases in the FORE-SCE 2005 dataset. While cropland area decreases in the FORE-SCE 2005 data, there is a widespread change from grassland to cropland in the western portion of the domain when compared with the MODIS data. Comparisons of the MODIS and FORE-SCE 2005 datasets with the Cropland Data Layer in Nebraska (CDL; https://www.nass.usda.gov/Research_and_Science/Cropland/SARS1a.php; South Dakota information is not available for 2005) show that the latter dataset matches most closely with the spatial distribution of grassland and cropland from the 2005 CDL. CDL has grassland extended much farther to the east in northern Nebraska and a larger extent of cropland in the southwest relative to MODIS. Thus, for this specific WRF domain, the FORE-SCE 2005 data present a more accurate depiction of LULC when compared with the MODIS data.

Comparison of the FORE-SCE 2005 data with the FORE-SCE 2050 data (Fig. 2) from the four modeled scenarios indicates distinct differences (Table 4). With the primary LULC types in the domain being grassland, hay/pasture, and cropland, the comparison is focused on those LULC categories. Grassland area decreases in the A1B (−22.6%), A2 (−9.10%), and B1 (−3.50%) scenarios and increases in the B2 (+4.11%) scenario. Cropland follows the same trend, except it increases in A1B (+13.5%), A2 (+8.20%), and B1 (+3.21%) scenarios and decreases in the B2 (−4.70%) scenario. Changes in hay/pasture include a large increase in the A1B (73.2%) scenario, an increase in the A2 (+1.92%) scenario, and decreases in the B1 (−6.68%) and B2 (−4.50%) scenarios. While other categories changed from 2005 to 2050, the only other category with a notable change is the developed class, which increased by around 85% and 90% in the A1B and A2 scenarios, respectively, 57% in the B1 scenario, and 43% in the B2 scenario.

As the primary LULC categories within the chosen WRF domain are cropland, grassland, and hay/pasture, it is important to note the model specific effects of changes between these LULC categories. Esteve (2016) and Cuntz et al. (2016) noted that there are numerous variables within the WRF modeling system static table input files that affect surface moisture transport and the radiation budget, vegetation height (HVT), the slope of the Ball–Woodrow–Berry stomatal conductance model (MP), soil moisture availability (SLMO), leaf reflectivity (RHOL), and stem reflectivity (RHOS). Esteve (2016) stated that emissivity, albedo, and soil moisture availability directly affect the partitioning of surface energy into latent and sensible heat fluxes. Cuntz et al. (2016) found that most vegetation-related parameters in WRF affect evapotranspiration (ET). Among these, evaporation was most strongly sensitive to HVT, while transpiration was strongly controlled by MP. Thus, albedo, emissivity, soil moisture availability, HVT, and MP are the variables of focus for this research. It is recognized, however, that the controls of ET are much more complex than those of the other variables and based on numerous biophysical and physical properties of plants and soils. The following discussion is solely related to variables within the Noah-MP land surface model used for our WRF modeling configuration.

While albedo and emissivity might be important to determining the surface radiation budget, their values are very close within the three dominant LULC categories (19%/0.96 for grassland, 18%/~0.96 for cropland, and 18%/~0.96 for hay/pasture). Soil moisture availability varies between the three categories, with grassland being the lowest at 0.15, hay/pasture being at 0.30, and cropland being at 0.5. Higher soil moisture availability means that the surface would produce closer to potential ET than it would with a lower value of soil moisture availability. While Cuntz et al. (2016) found that MP was a strong control of transpiration (thus ET) within the Noah-MP land surface model, the three categories mentioned here (grassland, cropland, and hay/pasture) all have the same MP value (9.0). Thus, while MP does produce a strong influence on plant transpiration within the model, it does not appear to be a factor within the LULCC present in these simulations.

HVT is different among the three LULC categories where grassland, hay/pasture, and cropland have values of 1.00, 1.5, and 2.00 m, respectively. Higher HVT would mean less surface-based evaporation owing to larger canopy density, in conjunction with the increased canopy interception by the taller vegetation. Thus, independent of other factors affecting ET, vegetation with higher heights would reduce overall evaporation (and thus ET) relative to vegetation with shorter heights. Thus, while the HVT increase would show that ET would be decreased, ET would increase for changes to cropland due to a much higher soil moisture availability and decreased albedo. Correspondingly, a switch to grassland would increase surface-based ET from lower vegetation density but decrease overall ET linked to a larger albedo and less transpiration from grass. Aside from the albedo effects, which would reduce or raise both surface heat fluxes, a reduced latent flux (ET) would lead to increased sensible heat flux and vice versa.

b. *Effects of FORE-SCE LULCC on near surface meteorology*

Overall, the change of LULC from the FORE-SCE 2005 historical LULC dataset to the FORE-SCE 2050 scenario

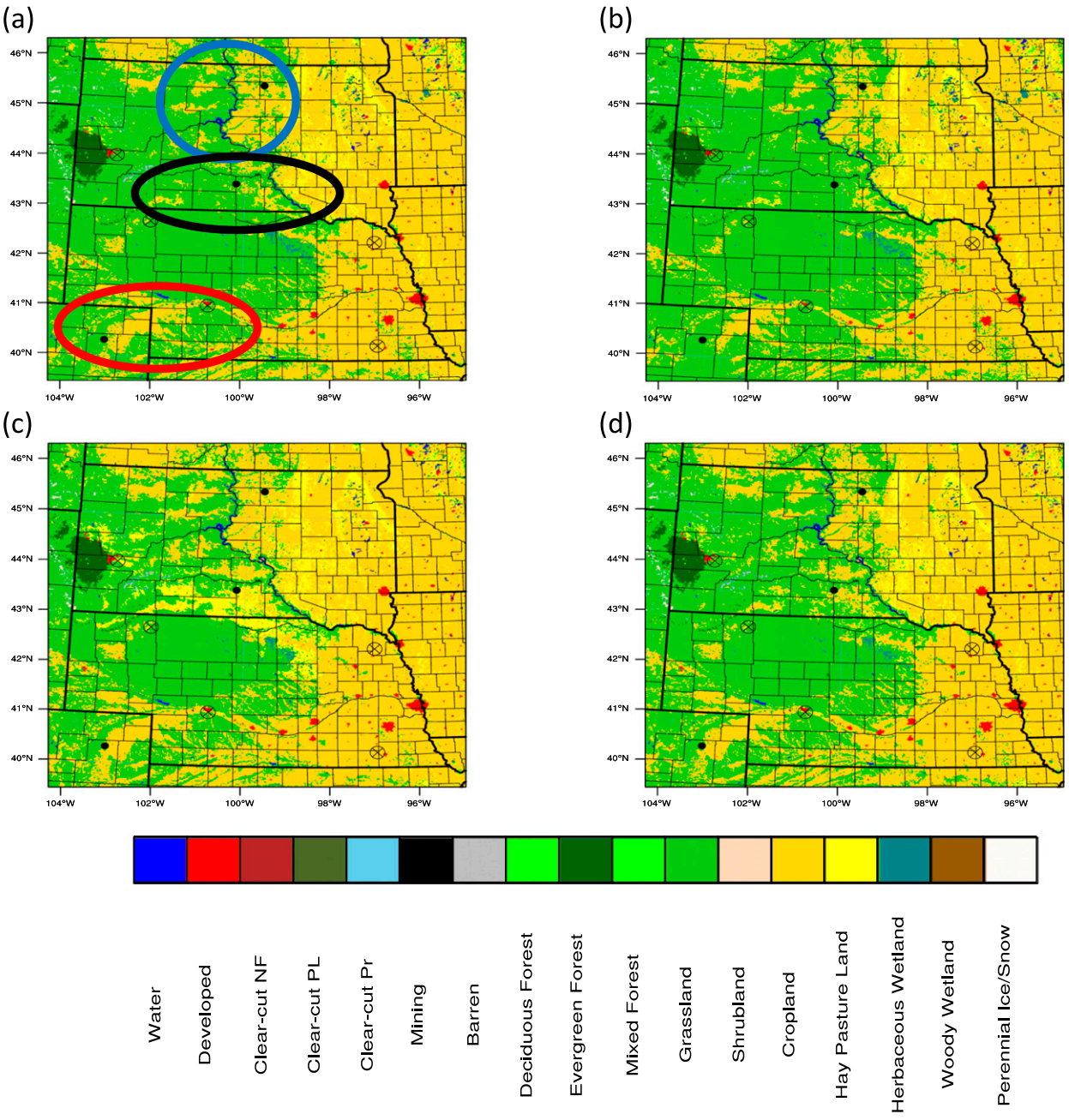

FIG. 2. FORE-SCE LULC for the (a) B1 scenario, (b) B2 scenario, (c) A1B scenario, and (d) A2 scenario. Also included are the location of the vertical profiles, as well as colored ovals [(a); colors match the vertical profile colors] highlighting the three main areas of change when comparing the FORE-SCE LULC datasets and the default WRF LULC dataset.

datasets caused nearly no average daytime or nighttime changes across the inner WRF domain for the 4 days used for simulations and analysis. Due to the localized nature of LULCC within the FORE-SCE dataset for 2050, the nature of the atmospheric differences is subtle. However, spatial patterns are detected through the analysis of the four WRF simulations completed using the four FORE-SCE 2050 LULCC scenarios.

The effect of LULCC, at least directly within WRF, would influence the surface radiative fluxes first and foremost. Thus, an analysis of sensible and latent heat flux differences is necessary to diagnose the effect of the FORE-SCE LULC dataset within WRF. However, separately diagnosing and comparing the fluxes is difficult, and thereby for this analysis an investigation of the Bowen ratio was used. The Bowen ratio is the ratio between sensible and latent heat fluxes, and thus an

TABLE 4. Gridpoint count of LULC types within the inner WRF domain. The three tundra classes in the MODIS category were removed because of no matching LULC type in FORE-SCE and no domain points in the control simulation being identified as tundra. Percent change is listed in parentheses after each gridpoint count value, and the sign indicates either an increase or decrease in the number of grid points.

Categories	MODIS	Historical 2005	A1B 2050	A2 2050	B1 2050	B2 2050
Water	1290	788	788 (0%)	785 (−0.38%)	798 (−1.27%)	804 (−2.03%)
Developed	150	701	1294 (84.6%)	1328 (89.4%)	1104 (57.5%)	1005 (43.4%)
Mechanically disturbed national forest	[a]	0	0	0	0	0
Mechanically disturbed public land	[a]	0	0	0	0	0
Mechanically disturbed private	[a]	0	0	0	0	0
Mining	[a]	1	1	1	1	1
Barren	24	125	142 (13.6%)	132 (5.6%)	124 (−0.8%)	119 (−4.8%)
Deciduous forest	17	581	451 (−22.4%)	440 (−24.3%)	595 (2.41%)	597 (2.75%)
Evergreen forest	1194	1805	1833 (1.55%)	1820 (0.83%)	1814 (0.50%)	1813 (0.44%)
Mixing forest	908	0	1	1	0	0
Grassland	54 727	69 308	53 869 (−22.6%)	63 004 (−9.10%)	66 912 (−3.50%)	72 161 (4.11%)
Shrubland	1062	546	329 (−39.7%)	427 (−21.8%)	435 (−20.3%)	485 (−11.2%)
Cropland	78 735	71 621	81 255 (13.5%)	77 496 (8.20%)	73 922 (3.21%)	68 258 (−4.70%)
Hay/pasture	15 890	7737	13 399 (73.2%)	7885 (1.92%)	7220 (−6.68%)	7351 (−4.50%)
Herbaceous wetland	[a]	702	578 (−17.7%)	625 (−11.0%)	978 (39.3%)	1299 (85.0%)
Woody wetland	[a]	85	60 (−29.4%)	56 (−34.1%)	97 (14.1%)	107 (25.9%)
Permanent wetland	1	[a]	[a]	[a]	[a]	[a]
Perennial ice/snow	0	0	0	0	0	0

[a] The LULC type is not available in that LULC dataset.

increase in sensible heat flux would increase the ratio, and an increase in latent heat flux would decrease the ratio. Still, this analysis is difficult given that the LULCC primarily occurs between grassland, cropland, and hay/pasture. This is because the Bowen ratio is small for these LULC types and hence, the differences occurring from LULCC and these LULC types are even smaller. Because most of the Bowen ratio values are between −5.0 and +5.0, we have masked out greater positive and negative values. Further, given the nature of surface radiation fluxes, nighttime differences were not analyzed for the Bowen ratio.

Spatially, the Bowen ratio differences are similar across all four FORE-SCE simulations (Fig. 3). Large-magnitude differences are seen across the southeastern portion of the WRF inner domain. These differences coincided with large differences found across all four scenarios. Within all four simulations, Bowen ratio differences are reflective of the LULCC. The B1 scenario (Fig. 3a), even with the smallest LULCC of the four scenarios, shows negative Bowen ratio differences resultant from grassland to cropland changes in northern South Dakota. The simulation for the B1 scenario shows positive Bowen ratio differences near the central Nebraska and South Dakota border resultant from cropland to grassland LULCC. The B2 scenario (Fig. 3b) is the only scenario with a marked decrease in cropland area within the WRF inner domain of the four FORE-SCE scenarios. This led to larger positive Bowen ratio differences within the primary LULCC areas relative to the other scenarios because of increased sensible heating and reduced ET. However, increases in cropland are still found across central South Dakota, resulting in negative Bowen ratio differences in this area.

The A1B scenario (Fig. 3c) depicts a large change from cropland and grassland to hay/pasture, primarily across the center of the WRF inner domain. The A1B Bowen ratio differences do show more positive differences across the South Dakota and Nebraska border, but otherwise the central portion of the domain shows difference signals similar to the other cases. This is likely due to the large similarities in WRF static variables for grassland and hay/pasture. Thus, LULCC between these two LULC categories would not have substantial effects as seen in the A1B scenario simulation. However, LULCC to cropland can be seen in northern South Dakota and southwestern Nebraska/northeastern Colorado, resulting in negative Bowen ratio differences. Last, in the A2 scenario (Fig. 3d), expansive areas of grassland are changed to cropland across central and western South Dakota and southwestern Nebraska and northeastern Colorado. This results in widespread negative differences, with a reduction of the positive differences relative to the other three FORE-SCE simulations.

The 2-m temperature field within the FORE-SCE WRF simulations (Fig. 4) are similar during the daytime (Figs. 4a–d) and nighttime (Figs. 4e–h). Widespread increases in surface temperature (0.5°–1°C) are observed across the inner domain during the daytime, with negative differences evident, but with substantially less coverage across the WRF inner domain. During the night, negative differences areas are more robust, with large spatial areas showing differences in the range from −0.5° to −1°C. While all four scenarios depict similar daytime and nighttime differences, the magnitudes of the differences exist in the primary LULCC areas. Both southwestern Nebraska and the bordering areas of north-central Nebraska and south-central South Dakota show negative difference

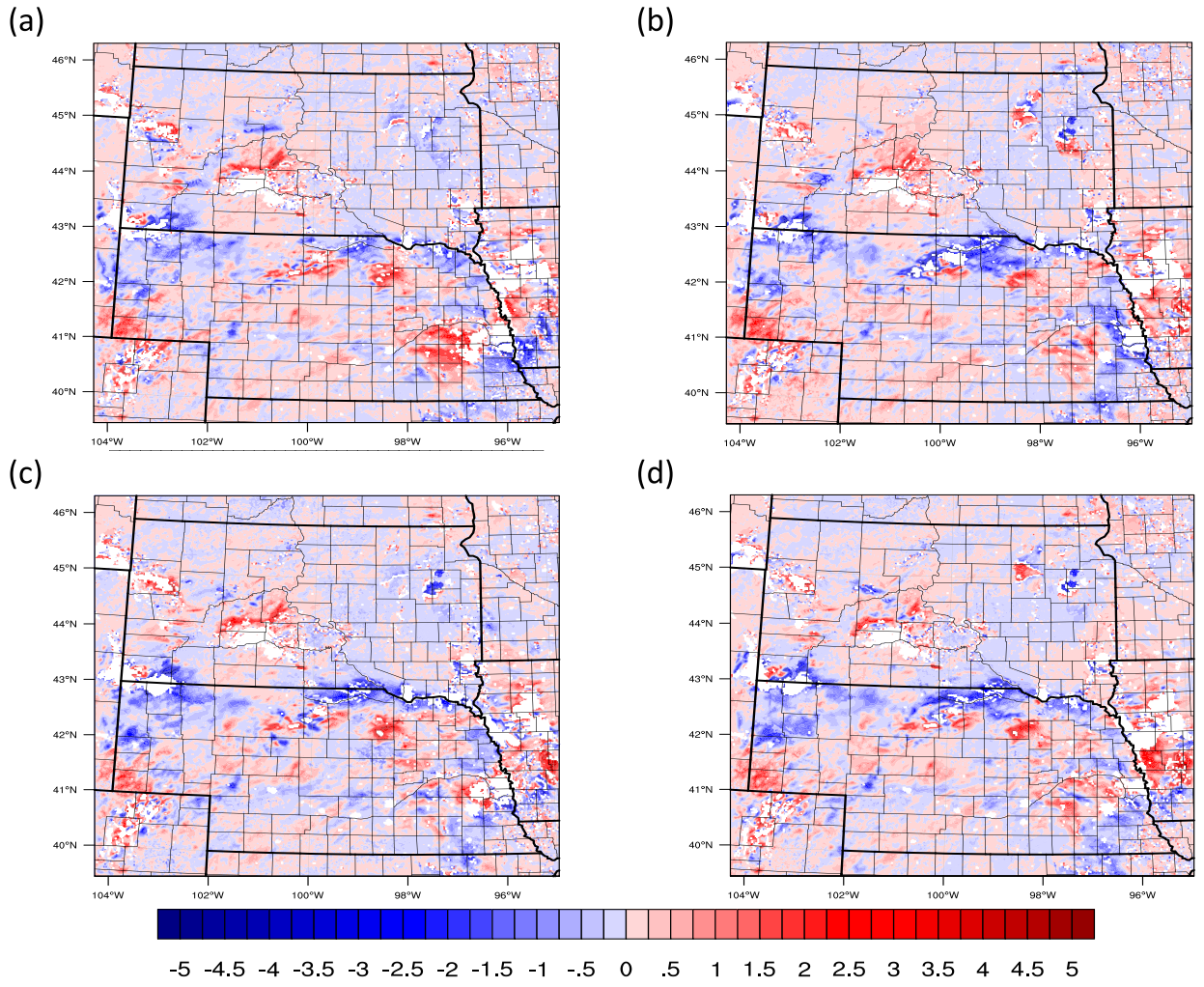

FIG. 3. WRF FORE-SCE Bowen ratio daytime (1200–0000 UTC) differences (FORE-SCE − Control) from the (a) B1 scenario, (b) B2 scenario, (c) A1B scenario, and (d) A2 scenario across the four simulation days analyzed. Bowen ratio differences are unitless. Differences were calculated as the FORE-SCE minus the Control WRF simulations prior to averaging over the four simulation days. Empty areas are values above 5 or below −5 that were masked out to facilitate an analysis of smaller value differences.

areas with the largest magnitude in the A1B scenario (Figs. 4c,g) and the smallest in the B1 scenario (Figs. 4a,e). While in central Nebraska and South Dakota, B2 scenario (Figs. 4b,f) shows more moderate negative temperature differences relative to A1B. Negative temperature differences outside of this area are much larger relative to the other three scenarios. The A2 scenario (Figs. 4d,h) shows a spatial pattern of temperature differences that are similar to those of the B2 scenario, except in eastern Nebraska. Here positive temperature differences are found during the daytime and nighttime as compared with the B2 scenario (which showed negative temperature differences in this same region). North-central South Dakota shows positive differences linked to the modification of grassland to cropland in each scenario.

With respect to surface moisture, the differences between the FORE-SCE and control simulations are similar for the day and night composites (Fig. 5) across the four different FORE-SCE scenarios. During the daytime (Figs. 5a–d), negative moisture differences (0.3–0.5 g kg^{-1}) dominate west-central South Dakota and Nebraska, broken up by two positive moisture difference areas originating in southwestern Nebraska and east-central South Dakota. Interestingly, while the B1 (Figs. 5a,e) and B2 (Figs. 5b,f) scenarios have the smallest increases of cropland area of the four scenarios, they show the largest positive moisture differences across the central portion of the domain, especially in southwestern Nebraska. Thus, the simulated increases in cropland depicted in the B1 and B2 scenarios are primarily contained in these two regions. The extreme eastern and western portions of the domain contain largely positive moisture differences, especially during the nighttime. This is especially important in the A1B (Figs. 5c,g) and A2 (Figs. 5d,h) scenarios, as the largest increase of agricultural (cropland and hay/pasture) area in these two scenarios appears to occur across the eastern border region of Nebraska and South Dakota (Fig. 2). Given the

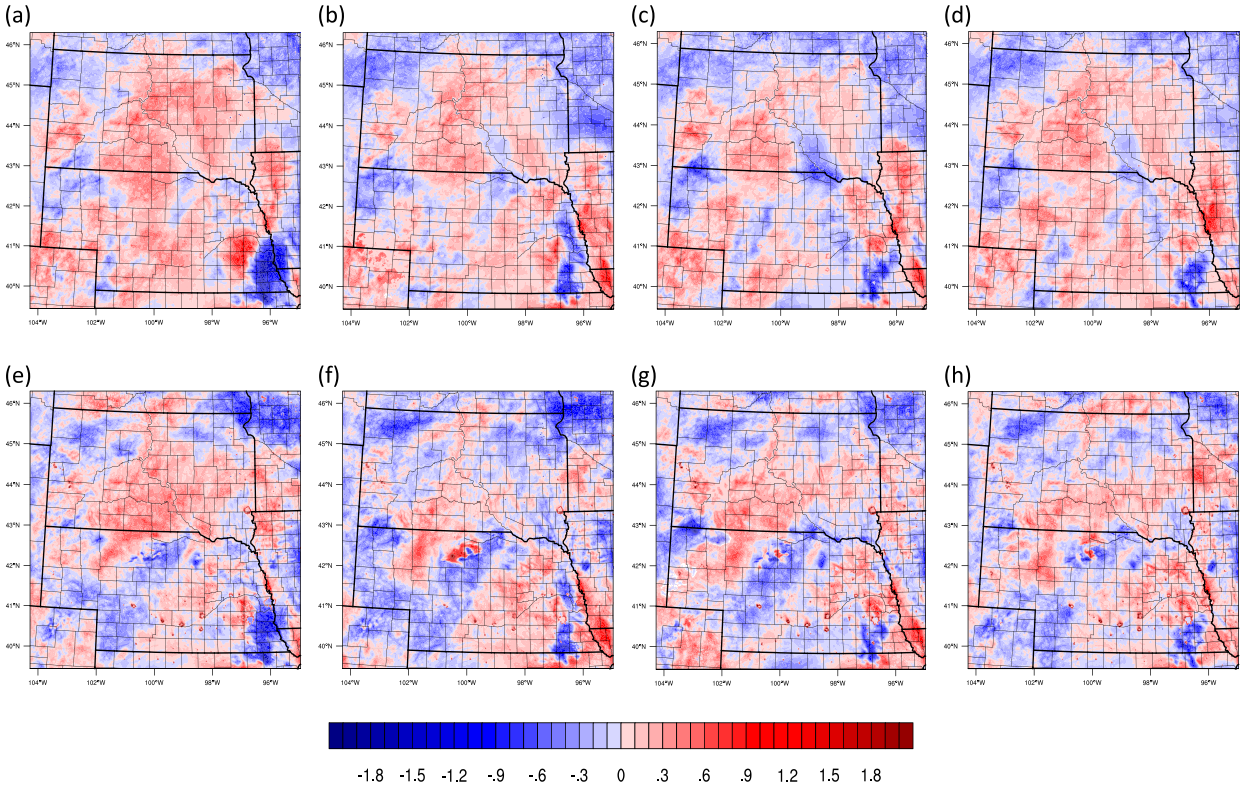

FIG. 4. WRF FORE-SCE 2-m daytime (1200–0000 UTC) temperature differences (°C; FORE-SCE − Control) from the (a) B1 scenario, (b) B2 scenario, (c) A1B scenario, and (d) A2 scenario across the four simulation days analyzed. (e)–(h) As in (a)–(d), but for the nighttime. Differences were calculated as the FORE-SCE minus the control WRF simulations prior to averaging over the three simulation days.

reduced magnitude of positive moisture differences is in southwestern Nebraska for the A1B and A2 scenarios, this moisture increase across the central portion of the domain appears linked to the increase of daytime and nighttime increases of moisture in the east-central portion of Nebraska and South Dakota. However, in three of the scenarios (B2, A1B, and A2) a negative moisture area is evident during the nighttime in the eastern portion of South Dakota likely linked to advection of low-level moisture from the north-central Nebraska–south-central South Dakota border. The areas of negative moisture differences in the southeastern portion of the domain during the daytime are not as robust or not as evident as in some scenarios for the nighttime composites. These areas of differences could be linked to the increase of urban area in southeastern Nebraska (Lincoln and Omaha, Nebraska) and a small area in southeastern Nebraska where croplands converted to grasslands in all scenarios. However, the area of positive differences in the eastern edge of the domain is difficult to explain with just the LULCC alone. No large-scale LULCC is noted within the four FORE-SCE future LULC datasets in this area. Hence, these large moisture differences in the eastern part of the domain could be caused by factors other than the LULCC.

Last, wind speed would be directly affected by the LULCC. Different LULC types have different roughness characteristics, which produces different levels of drag on the wind. Thus, LULCC would directly affect the wind across the WRF domains. Across all four scenarios (Fig. 6) wind speeds increased in the western portion of the domain and decreased in the east. Nighttime differences were nearly identical across each of the scenarios and thus only the daytime differences were analyzed for this study. In the B1 scenario simulation (Fig. 6a), LULCC in the center of domain caused small magnitude increases in the wind speed due to increases of grassland area, which resulted in decreased the surface roughness. In northern South Dakota, the decreased wind speeds are possibly linked to the increase of cropland area. In the B2 scenario (Fig. 6b), the large increase of grassland at the expense of cropland area is evident in the widespread increases in wind speeds across the western portion of the WRF inner domain. Small, negative differences are found in the southwestern portion of the domain and in extreme western South Dakota under all four FORE-SCE scenario simulations.

In the A1B scenario (Fig. 6c), wind speed increases and decreases are not as large in magnitude as the other scenario simulations. This is likely caused by the more widespread change of grassland/cropland to hay/pasture within this scenario. This expanded the negative wind speed differences in south-central South Dakota toward the west given the expanse of new hay/pasture area within this scenario. The more varied wind speed differences are likely caused by the change from

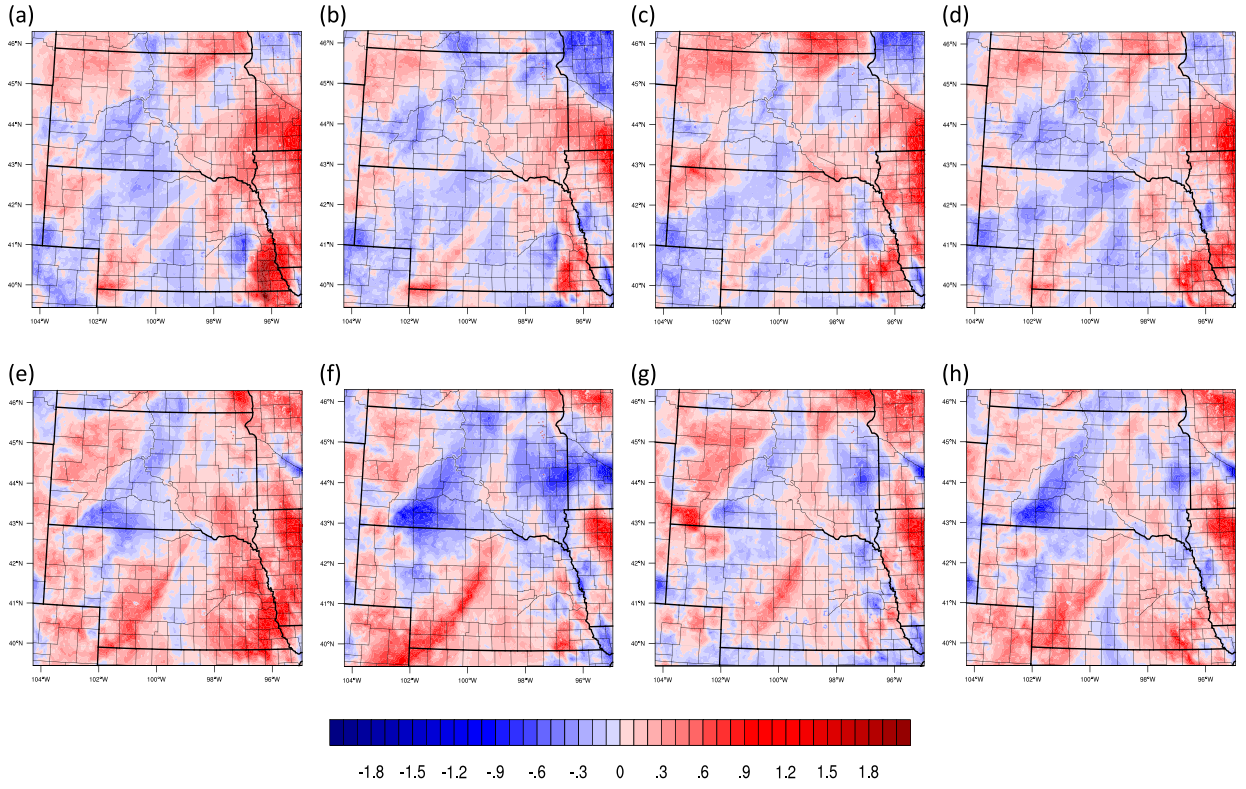

FIG. 5. WRF FORE-SCE daytime (1200–0000 UTC) 2-m specific humidity differences (g kg^{-1}; FORE-SCE − Control) from the (a) B1 scenario, (b) B2 scenario, (c) A1B scenario, and (d) A2 scenario across the four simulation days analyzed. (e)–(h) As in (a)–(d), but for the nighttime. Differences were calculated as the FORE-SCE minus the control WRF simulations prior to averaging over the three simulation days.

both grassland and cropland to hay/pasture. This would cause both increases (change from cropland to grassland) and decreases (change from grassland to cropland) in wind speed, as the surface roughness has changed. Unlike the other variables, wind speed could be affected across the entire domain from smaller changes in LULC. Large-scale shifts in the inner domain, especially given the spatial patterns (differences appear oriented form southwest to northeast) of the differences, are likely linked to changing surface roughness due to discrete changes in LULC near the origin point of the banded differences in 10-m wind speed. The A2 scenario (Fig. 6d) simulation resulted in the largest negative wind speed differences of the four FORE-SCE simulations. This is likely caused by the location of the large cropland expansion within the A2 scenario. For example, the cropland expansion is more dominant in the northern portion of the domain (central and western South Dakota) relative to the other scenarios that noted increases of cropland in southwestern Nebraska. Subsequently, negative differences in wind speed in central and western South Dakota are found.

c. Effects of FORE-SCE LULCC on PBL evolution

Identifying the response of the PBL to the FORE-SCE LULCC would further assist in improving our understanding of these effects, especially on the convective environment. In this context PBLH is important for several convective processes (Wisse and Vilà-Guerau de Arellano 2004; Esau and Zilitinkevich 2010; Gentine et al. 2013). Like the other variables, PBLH differences (Fig. 7) are scattered and nonuniform across most of the domain. For all four scenarios, positive daytime and nighttime PBLH differences are evident across central South Dakota and eastern and western Nebraska. Negative PBLH differences are found in western South Dakota, extreme western Minnesota, northwestern Nebraska, and southeastern Nebraska. Daytime positive PBLH differences across central South Dakota in the B1 (Fig. 7a), B2 (Fig. 7b), and A2 (Fig. 7d) scenarios are similar while the A1B (Fig. 7c) scenario shows reduced area and magnitude of positive PBLH differences relative to the other three scenarios. The A1B scenario (Fig. 7c) also shows a larger area of negative PBLH differences along the eastern border region between Nebraska and South Dakota and coincided with large negative temperature differences evident only in the A1B scenario. While all four scenarios show a series of negative PBLH difference areas across central and southwestern Nebraska, they are larger in magnitude in the A1B scenario than in the other three scenarios. The differences shown in the PBLH field relate more closely to the temperature differences in Fig. 4, showing the relation between LULCC and the radiation balance at the surface. Different LULC types would affect balance of sensible

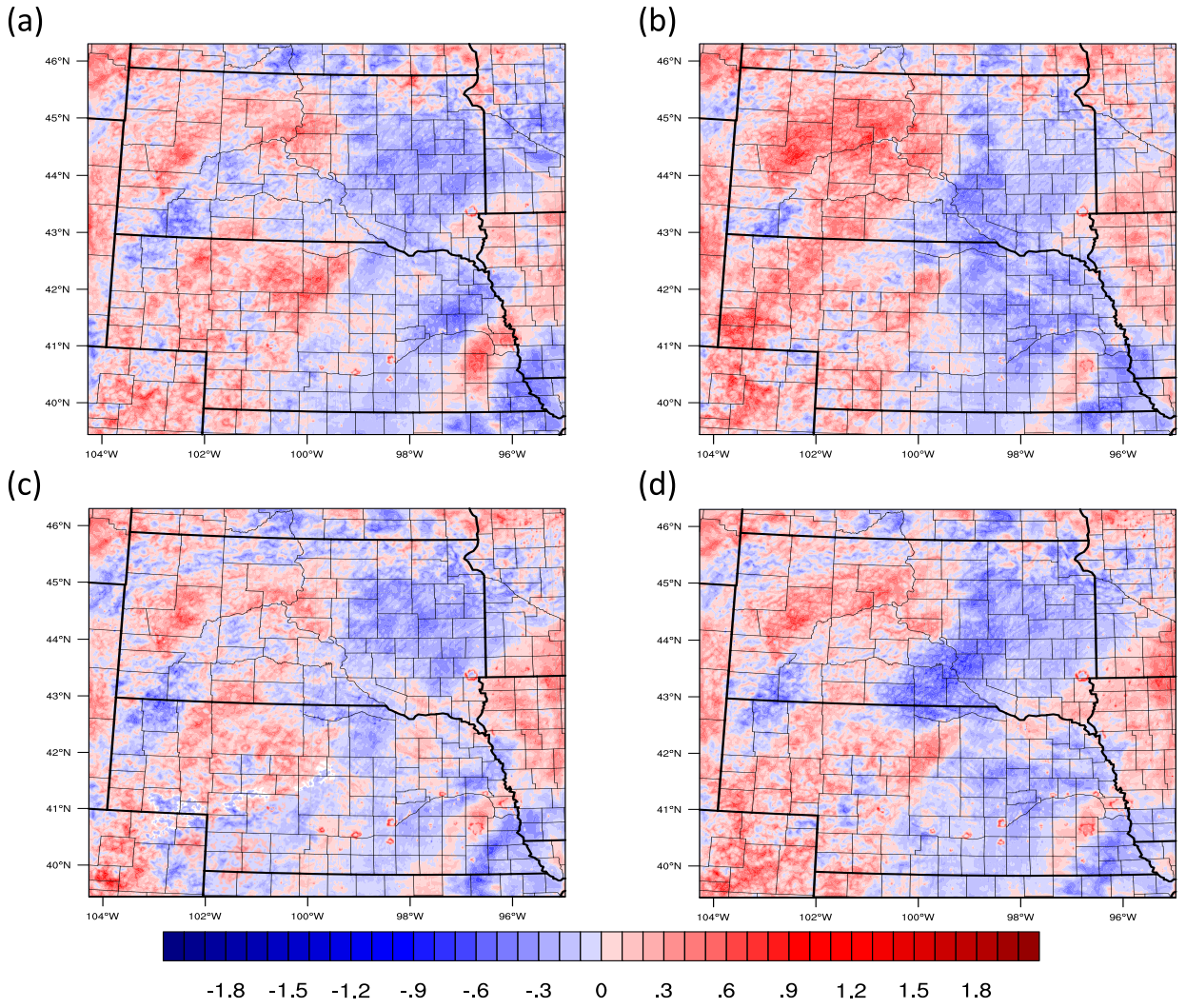

FIG. 6. WRF FORE-SCE daytime (1200–0000 UTC) 10-m wind speed differences (m s^{-1}; FORE-SCE − Control) from the (a) B1 scenario, (b) B2 scenario, (c) A1B scenario, and (d) A2 scenario across the four simulation days analyzed. Differences were calculated as the FORE-SCE minus the Control WRF simulations prior to averaging over the four simulation days.

and latent heat fluxes at the surface. Increases in the sensible heat flux would increase turbulent kinetic energy in the simulation, thus increasing PBLH, with a decrease in the sensible heat flux leading to reduced PBLH. Owing to the surface radiative balance, decreases in the sensible heat flux would increase the latent heat flux, leading to moist conditions in the PBL. Both of these scenarios can foster or inhibit convective processes (Findell and Eltahir 2003a,b). For example, the lower PBLH could reduce the maximum achievable height of parcels below that of the level of free convection and lifting condensation level, thus making it harder for air parcels to become positively buoyant (Mahmood et al. 2011; Gentine et al. 2013; Zaitchik et al. 2013). However, if the decreased PBLHs are caused by decreases in the sensible heat flux and thus, increased latent heat flux and PBL moisture, which also increases moist static energy, the PBLH difference could be conducive to enhanced convection (e.g., Eltahir 1998; Findell and Eltahir 1999).

While differences in other atmospheric fields have been found, the CAPE is relatively unchanged (Fig. 8). During the day, an area in southwestern Nebraska shows larger positive differences (100–200 J kg^{-1}) under the A2 (Figs. 8d,h), B1 (Figs. 8a,e), and B2 (Figs. 8b,f) scenarios. While a positive CAPE difference region is evident for A1B scenario (Figs. 8c,g), it is of reduced magnitude relative to the CAPE differences found in the other three scenarios. These differences are associated with positive temperature and moisture differences, which would aid in creating a more favorable environment for convection. On the other hand, this is not evident during the night when the central and western portion of the domain primarily show small negative differences across all four scenarios. Large CAPE differences are evident in each scenario in the far eastern portion of the domain during the day and night, likely linked to large increases in moisture shown in Fig. 5.

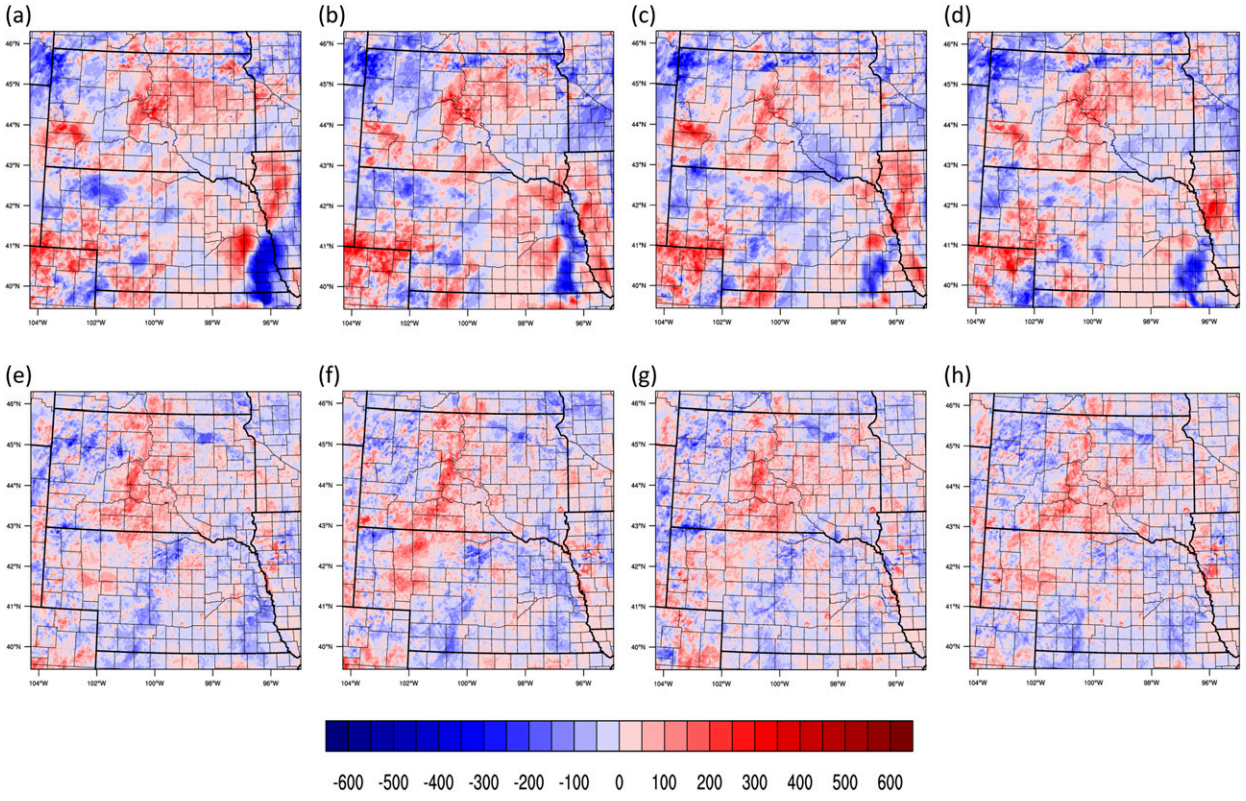

FIG. 7. WRF FORE-SCE daytime (1200–0000 UTC) PBLH differences (m; FORE-SCE − Control) from the (a) B1 scenario, (b) B2 scenario, (c) A1B scenario, and (d) A2 scenario across the four simulation days analyzed. (e)–(h) As in (a)–(d), but for the nighttime. Differences were calculated as the FORE-SCE minus the control WRF simulations prior to averaging over the three simulation days.

Analysis of the vertical differences in temperature and dewpoint temperature helps to understand how surface changes influence the convective environment within the PBL (lowest 2–4 km of the vertical plots). The results show that changes are more pronounced in the near-surface (Fig. 9) for temperature (Figs. 9a,b) than in the moisture fields (Figs. 9c,d). Further, the temperature profiles show much more variability in differences between scenarios than do those of moisture. It is found that during the day, both locations X and Y show positive near-surface temperature differences (Fig. 9a) coincident with small negative differences in the near-surface moisture field (Fig. 9c). Location Z presents more varied results with scenarios B1 and B2 showing positive and A1B and A2 negative differences in temperature. The near-surface moisture differences at location Z are varied as well, with scenarios B1 and A1B demonstrating positive differences and scenarios B2 and A2 negative.

4. Discussion

Our results indicate that all four FORE-SCE modeled LULCC scenarios affected the WRF simulations in predictable manners. Across the study area (inner WRF domain), there are three primary areas of LULCC: southwestern Nebraska (cropland to grassland area in B2, increases in grassland from cropland in the other 3), north-central Nebraska and south-central South Dakota (grassland to hay/pasture and cropland area), and north-central South Dakota (grassland to cropland area) (Figs. 1b and 2). All three of these areas showed distinct surface flux effects from the noted LULCC. Bowen ratio differences (Fig. 3) were reflective of the noted LULCC across all four FORE-SCE scenario simulations. Increases of grassland or hay/pasture area (at the expense of cropland) resulted in widespread positive Bowen ratio differences across all four scenario simulations, while increases in cropland (at the expense of grassland and/or hay/pasture) resulted in negative Bowen ratio differences.

While factors besides LULCC can affect surface fluxes (clouds, extra input water, wind, etc.), the specific chosen date was used to minimize the influence of such features. While clouds were evident within the simulations, these were primarily found in the extreme western and eastern portion of the domain. Both regions experienced large-magnitude Bowen ratio differences across the four scenario simulations, thus were not included within our analysis of Bowen ratio. Precipitation did not occur within our simulations, and thus this would not have affected the surface fluxes. Differences in vegetation height, and thus different roughness lengths, is noted with differing LULC types and thus affecting wind speeds. This likely explains the banded and large-scale structures found in the 10-m wind speed differences across all four scenarios, as changes in roughness lengths across discrete areas could affect wind speeds downwind

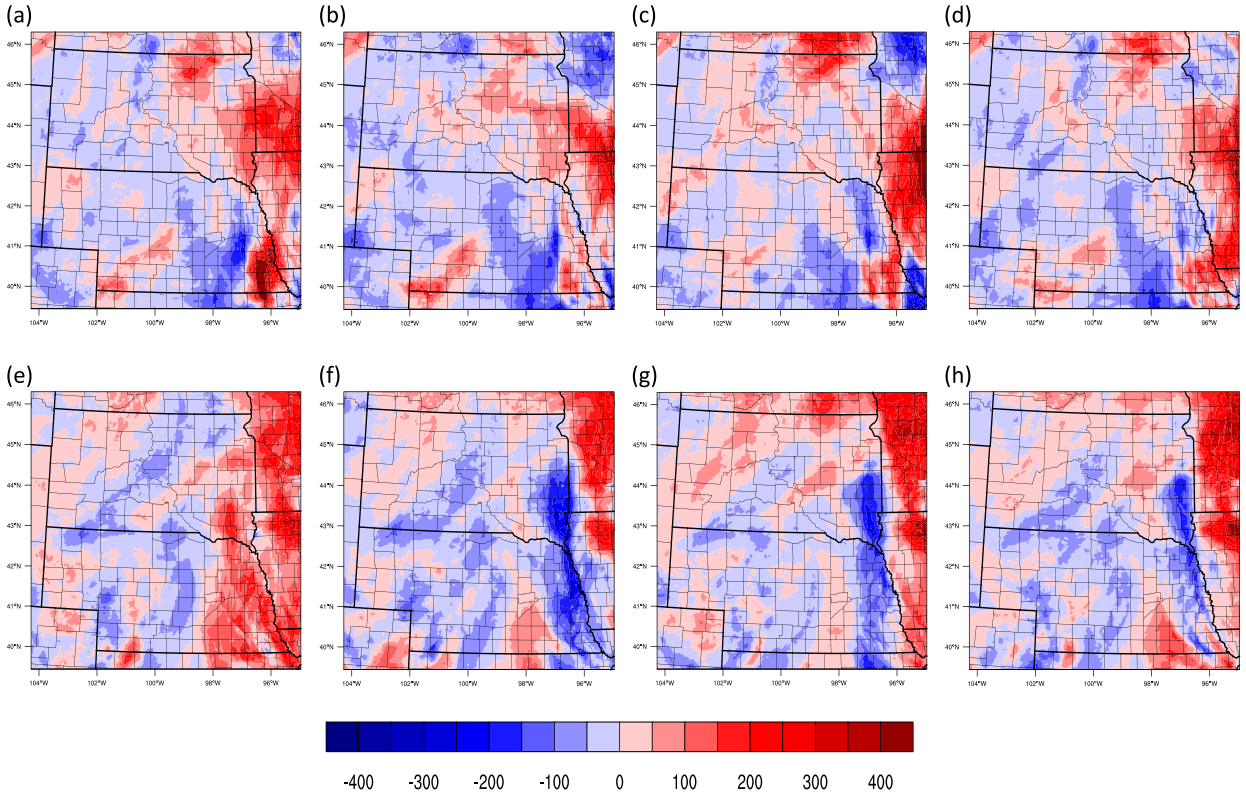

FIG. 8. WRF FORE-SCE daytime (1200–0000 UTC) CAPE differences (J kg^{-1}; FORE-SCE − Control) from the (a) B1 scenario, (b) B2 scenario, (c) A1B scenario, and (d) A2 scenario across the four simulation days analyzed. (e)–(h) As in (a)–(d), but for the nighttime. Differences were calculated as the FORE-SCE minus the control WRF simulations prior to averaging over the three simulation days.

of the initial cause of the change. Given the spatial structure (differences oriented from southwest to northeast) within the wind speed differences (Fig. 6), this is likely the primary cause of the widespread wind speed differences. For example, increasing agricultural (cropland or hay/pasture) area at the expense of grassland across the central Nebraska–South Dakota border area and central South Dakota would increase the roughness length, decreasing wind speeds and explaining the widespread negative differences seen in most of eastern South Dakota. A change from grassland to cropland would lower wind speeds and vice versa. As with the Bowen ratio shifts, changes to cropland area slowed winds across the southwestern Nebraska and northeastern Colorado and across the south-central and northern South Dakota LULCC regions.

Across north-central Nebraska and south-central South Dakota, daytime temperatures decrease (from −0.3° to −1°C; Figs. 4a–d) and moisture content increases (0.3–0.5 g kg^{-1}; Figs. 5a–d), especially in central South Dakota along the Missouri River. During the nighttime, temperatures are increased (0.3°–0.5°C; Figs. 4e–h) in this same area, due to the increase of moisture (0.1–0.3 g kg^{-1}; Figs. 5e–h) lowering the local diurnal temperature range. In north-central South Dakota, changes from grassland to cropland have locally increased moisture (0.3–0.5 g kg^{-1}) and decreased temperatures (from −0.3° to −0.6°C). This area shows varied extent of LULCC depending on the scenario and thus the degree of change is different for each, with B1 showing the least change and A1B showing the greatest. An area showing increases in temperature (0.3°–0.5°C) and decreases in moisture (from −0.3 to −0.5 g kg^{-1}) is evident near south-central South Dakota. It is opposite of what is expected given the LULCC (grassland to cropland) in north-central South Dakota. This area of increased temperature and reduced moisture appears to be connected with an area across the western Nebraska and South Dakota border, and thus is likely related to advection in the region. As noted previously, the most notable area of atmospheric response to LULCC within the FORE-SCE simulations is found in southwestern Nebraska (cropland to grassland in B2, small changes between cropland and grassland in the other three scenarios). Positive temperature differences are widespread during the daytime (0.3°–0.5°C), and negative temperature differences (from −0.5° to −0.7°C) dominate the area during the night. These are collocated with primarily negative moisture differences during the daytime (from −0.1 to −0.3 g kg^{-1}) and positive moisture difference during the nighttime (0.3–1.0 g kg^{-1}), which would result in the positive temperature differences depicted during the day and night. However, small areas in southwestern Nebraska show positive moisture differences during the day (0.1–0.5 g kg^{-1}), which are linked to the larger positive moisture difference areas at night. It appears that with

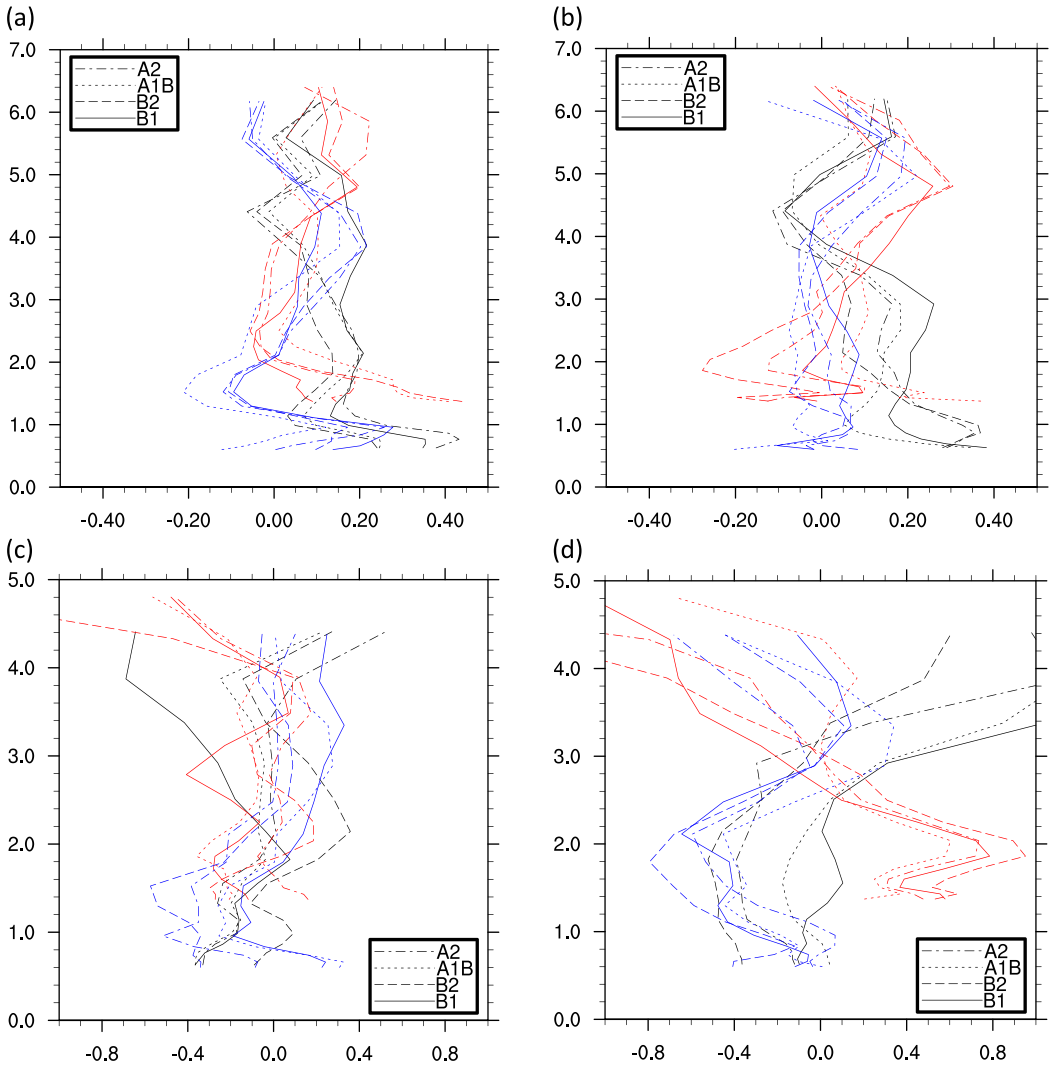

FIG. 9. Vertical profiles of (a) daytime temperature differences (FORE-SCE − Control), (b) nighttime temperature differences, (c) daytime dewpoint differences, and (d) nighttime dewpoint differences across all four simulation days. Daytime is from 1200 to 0000 UTC, and nighttime is from 0000 to 1200 UTC. Temperature and dewpoint temperature differences are in degrees Celsius. The blue line represents data taken from location Z, the black line represents data taken from location Y, and the red line represents data taken from location X as represented in Fig. 1b.

increasing grassland, the primary moisture source (agricultural land) in the region shifted to the east. This resulted in increases in CAPE, signaling a more favorable convective environment in southwest Nebraska, just east of the primary area of LULCC.

The differences at the surface also affected the simulated atmosphere above the surface, typically in line with the noted LULCC. For example, the location X (Fig. 9; red lines) reports changes from cropland to grassland (in B2, with some change over from cropland to grassland; for the other three scenarios, changes across very small areas) and a resulting warmer and drier environment (Figs. 9a,c). However, all of the three primary LULCC areas within our domain were not affected in line with the analyzed LULCC within the FORE-SCE dataset. At location Y (Fig. 9; black lines), grassland is changed to cropland (A2 and B1), hay/pasture (A1B), or no change (B2). Interestingly, location Y depicts consistent daytime differences for all four scenarios. Location Z (Fig. 9; blue lines) shows LULCC from grassland to cropland for all four scenarios but does not show consistent lower tropospheric differences during the day or night.

Overall, it is found that many of the differences in the simulations are in line with the conceptual understanding of land–atmosphere interactions and previous LULCC effects research (e.g., Pielke et al. 2011; Mahmood et al. 2014). In a modeling study, Bounoua et al. (2000) showed that surface temperature decreased on average 1.8 K at the peak of the growing season

(June, July, and August) owing to LULCC from a drier surface to one with higher evapotranspiration in the mid- and higher latitudes. Further, Adegoke et al. (2007) used the Regional Atmospheric Modeling System to show that a drier (nonirrigated) surface over Nebraska led to a warming of 1.4°C relative to their wet and control (with irrigation) simulations. Even though the differences in magnitudes in this study are lower than in previous modeling studies, the previous studies focus on more extreme variations in LULCC, which led to stronger modifications in near-surface atmospheric variables. Thus, although this study utilizes a different modeling system, the results of this study still largely agree with the results from previous modeling studies.

5. Conclusions

Substantial LULCC across the central United States has already taken place and is predicted to continue due to socioeconomic needs and policies resulting from population growth and climate change. The effects of LULCC, especially the change from natural to agricultural land, over the last century in the central United States has modified the natural climate of the region and notably affected near-surface temperature and moisture and thus influenced the convective environment. As LULCC continues, investigations of the effects of estimated future LULC are warranted. This research is an introductory study of the use of four FORE-SCE simulated future LULCC scenario datasets to simulate their effects on the near-surface atmosphere and PBL. The FORE-SCE model used four IPCC scenarios, including the A1B, A2, B1, and B2 scenarios, to develop four LULCC datasets from 2006 to 2100. The WRF Model is applied to determine potential effects of these future LULCC scenarios on the WRF simulated atmosphere. Five simulations were conducted where one was a control run with default LULC (2005 LULC from the FORE-SCE dataset) while the other four WRF simulations utilized four different projected 2050 LULCC scenarios from the FORE-SCE dataset. For each simulation, the first 3 days are considered as spinup/dynamic adjustment for the WRF Model and not included in the analysis. Data from the subsequent four days are used for this study. Results show the following:

- Across the southwestern portion of the study domain, a substantial area of cropland is changed to grassland in the B2 scenario, with small changes from cropland to grassland in the other three scenarios, leading to localized daytime surface warming and increased moisture toward the south.
- Across the central section of the study domain, an area of grassland is changed to agricultural land, leading to localized surface cooling and moistening.
- Across the north-central portion of the domain, an area of LULCC is transformed from grassland to cropland, leading to localized surface cooling and moistening.
- In the southwestern part of the domain, increases in CAPE resulted in a more convectively favorable environment in the B1 and B2 scenarios.
- In the A1B and A2 scenarios, increases of CAPE resulted in a more conditionally unstable convective environment in the southwest.

Overall, it was found that including the future LULCC would result in modification of simulated atmospheric variables and the convective environment across Nebraska and South Dakota during a quiescent summer period. These changes agree with the effects of observed LULCC across this region, noted in other studies. While these results represent a single model configuration, the atmospheric response found using the four FORE-SCE projected LULCC scenarios agrees with the theoretical understanding of land–atmosphere interactions due to modifications of grassland, cropland and pasture and thus would likely be reproducible for other model configurations. However, with this study representing a proof-of-concept method and without modifications to soil moisture pertaining to the new LULC categories, the results represent a less than robust analysis of the effects of future LULCC in the region.

A next step within this theme of research is planned to utilize the WRF modeling system and FORE-SCE dataset to investigate longer temporal period simulations and the effect of future LULCC on seasonal precipitation and hydroclimate evolution. Results would help guide stakeholders and local and regional decision-makers in creating reasonable goals to prepare for future climate changes linked to LULCC.

Acknowledgments. The authors thank two anonymous reviewers and the editor for their valuable comments that improved this paper. We also thank the USGS/EROS Center for providing and hosting the data (https://doi.org/10.5066/P95AK9HP; Sohl et al. 2018) that made this project possible. Funding for this project is provided by the High Plains Regional Climate Center (HPRCC) and Institute of Agriculture and Natural Resources, both at the University of Nebraska–Lincoln. This work was completed while the primary author was working at the HPRCC. Rezaul Mahmood acknowledges funding from the NSF Grant AGS-1853390. This work was completed utilizing the Holland Computing Center of the University of Nebraska, which receives support from the Nebraska Research Initiative. Any use of trade, firm, or product names is for descriptive purposes only and does not imply endorsement by the U.S. government.

REFERENCES

Adegoke, J. O., R. Pielke, and A. M. Carleton, 2007: Observational and modeling studies of the impacts of agriculture-related land use change on planetary boundary layer processes in the central US. *Agric. For. Meteor.*, **142**, 203–215, https://doi.org/10.1016/j.agrformet.2006.07.013.

Aegerter, C., and Coauthors, 2017: Mesoscale modeling of the meteorological impacts of irrigation during the 2012 central plains drought. *J. Appl. Meteor. Climatol.*, **56**, 1259–1283, https://doi.org/10.1175/JAMC-D-16-0292.1.

Bierwagen, B. G., D. M. Theobald, C. R. Pyke, A. Choate, P. Groth, J. V. Thomas, and P. Morefield, 2010: National housing and impervious surface scenarios for integrated climate impact assessments. *Proc. Natl. Acad. Sci. USA*, **107**, 20 887–20 892, https://doi.org/10.1073/pnas.1002096107.

Bonan, G. B., R. S. DeFries, M. T. Coe, and D. S. Ojima, 2004: Land use and climate. *Land Change Sciences*, G. Gutman et al., Eds., Kluwer Academic, 301–314.

Bounoua, L., G. J. Collatz, S. O. Los, P. J. Sellers, D. A. Dazlich, C. J. Tucker, and D. A. Randall, 2000: Sensitivity of climate to changes in NDVI. *J. Climate*, **13**, 2277–2292, https://doi.org/10.1175/1520-0442(2000)013<2277:SOCTCI>2.0.CO;2.

Broxton, P. D., X. Zeng, D. Sulla-Menashe, and P. A. Troch, 2014: A global land cover climatology using MODIS data. *J. Appl. Meteor. Climatol.*, **53**, 1593–1605, https://doi.org/10.1175/JAMC-D-13-0270.1.

Chen, L., and P. A. Dirmeyer, 2017: Impacts of land-use/land-cover change on afternoon precipitation over North America. *J. Climate*, **30**, 2121–2140, https://doi.org/10.1175/JCLI-D-16-0589.1.

——, ——, A. Tawfik, and D. M. Lawrence, 2017: Sensitivities of land cover–precipitation feedback to convective triggering. *J. Hydrometeor.*, **18**, 2265–2283, https://doi.org/10.1175/JHM-D-17-0011.1.

Costa, M. H., S. N. M. Yanagi, P. J. O. P. Souza, A. Ribeiro, and E. J. P. Rocha, 2007: Climate change in Amazonia caused by soybean cropland expansion, as compared to caused by pastureland expansion. *Geophys. Res. Lett.*, **34**, L07706, https://doi.org/10.1029/2007GL029271.

Cuntz, M., J. Mai, L. Samaniego, M. Clark, V. Wulfmeyer, O. Branch, S. Attinger, and S. Thober, 2016: The impact of standard and hard-coded parameters on the hydrologic fluxes in the Noah-MP land surface model. *J. Geophys. Res. Atmos.*, **121**, 10 676–10 700, https://doi.org/10.1002/2016JD025097.

Eltahir, E. A. B., 1998: A soil moisture rainfall feedback mechanism: 1: Theory and observations. *Water Resour. Res.*, **34**, 765–776, https://doi.org/10.1029/97WR03499.

EPA, 1999: Level III ecoregions of the continental United States. U.S. Environmental Protection Agency, National Health and Environmental Effects Research Laboratory, accessed 10 December 2019, https://www.epa.gov/eco-research/level-iii-and-iv-ecoregions-continental-united-states.

Esau, I., and S. Zilitinkevich, 2010: On the role of the planetary boundary layer depth in the climate system. *Adv. Sci. Res.*, **4**, 63–69, https://doi.org/10.5194/asr-4-63-2010.

Esteve, B. J., 2016: Land use influence in WRF model. A high resolution mesoscale modeling over Oriental Pyrenees. M.S. thesis, Faculty of Physics, University of Barcelona, 25 pp., http://diposit.ub.edu/dspace/bitstream/2445/105800/1/TFM_Bernat_Jimenez.pdf.

Fahey, D. W., S. J. Doherty, K. A. Hibbard, A. Romanou, and P. C. Taylor, 2017: Physical drivers of climate change. *Climate Science Special Report: Fourth National Climate Assessment*, Vol. I, D. J. Wuebbles et al., Eds., U.S. Global Change Research Program, 73–113, https://doi.org/10.7930/J0513WCR.

Findell, K. L., and E. A. B. Eltahir, 1999: Analysis of the pathways relating soil moisture and subsequent rainfall in Illinois. *J. Geophys. Res.*, **104**, 31 565–31 574, https://doi.org/10.1029/1999JD900757.

——, and ——, 2003a: Atmospheric controls on soil moisture–boundary layer interactions. Part I: Framework development. *J. Hydrometeor.*, **4**, 552–569, https://doi.org/10.1175/1525-7541(2003)004<0552:ACOSML>2.0.CO;2.

——, and ——, 2003b: Atmospheric controls on soil moisture–boundary layer interactions. Part II: Feedbacks within the continental United States. *J. Hydrometeor.*, **4**, 570–583, https://doi.org/10.1175/1525-7541(2003)004<0570:ACOSML>2.0.CO;2.

——, A. Berg, P. Gentine, J. P. Krasting, B. R. Lintner, S. Malyshev, J. A. Santanello Jr., and E. Shevliakova, 2017: The impact of anthropogenic land use and land cover change on regional climate extremes. *Nat. Commun.*, **8**, 989, https://doi.org/10.1038/s41467-017-01038-w.

Friedl, M. A., and Coauthors, 2002: Global land cover mapping from MODIS: Algorithms and early results. *Remote Sens. Environ.*, **83**, 287–302, https://doi.org/10.1016/S0034-4257(02)00078-0.

Garcia-Carreras, L., D. J. Parker, C. M. Taylor, C. E. Reeves, and J. G. Murphy, 2010: Impact of mesoscale vegetation heterogeneities on the dynamical and thermodynamic properties of the planetary boundary layer. *J. Geophys. Res.*, **115**, D03102, https://doi.org/10.1029/2009JD012811.

Ge, J. J., J. G. Qi, B. M. Lofgren, N. Moore, N. Torbick, and J. M. Olson, 2007: Impacts of land use/cover classification accuracy on regional climate simulations. *J. Geophys. Res.*, **112**, D05107, https://doi.org/10.1029/2006JD007404.

Gentine, P., A. A. M. Holtslag, F. D'Andrea, and M. Ek, 2013: Surface and atmospheric controls on the onset of moist convection over land. *J. Hydrometeor.*, **14**, 1443–1462, https://doi.org/10.1175/JHM-D-12-0137.1.

Harding, K. J., and P. K. Snyder, 2012a: The atmospheric response to irrigation in the Great Plains. Part II: The precipitation of irrigated water and changes in precipitation recycling. *J. Hydrometeor.*, **13**, 1687–1703, https://doi.org/10.1175/JHM-D-11-099.1.

——, and ——, 2012b: Modeling the atmospheric response to irrigation in the Great Plains. Part I: General impacts on precipitation and the energy budget. *J. Hydrometeor.*, **13**, 1667–1686, https://doi.org/10.1175/JHM-D-11-098.1.

Homer, C., and Coauthors, 2007: Completion of the 2001 National Land Cover Database for the coterminous United States. *Photogramm. Eng. Remote Sens.*, **73**, 337–341.

Huber, D., D. Mechem, and N. Brunsell, 2014: The effects of Great Plains irrigation on the surface energy balance, regional circulation, and precipitation. *Climate*, **2**, 103–128, https://doi.org/10.3390/cli2020103.

Jimenez, P. A., J. V.-G. de Arellano, J. Navarro, and J. F. Gonzalez-Rouco, 2014: Understanding land–atmosphere interactions across a range of spatial and temporal scales. *Bull. Amer. Meteor. Soc.*, **95**, ES14–ES17, https://doi.org/10.1175/BAMS-D-13-00029.1.

Justice, C. O., J. R. G. Townshend, E. F. Vermote, E. Masuoka, R. E. Wolfe, N. Saleous, D. P. Roy, and J. T. Morisette, 2002: An overview of MODIS Land data processing and product status. *Remote Sens. Environ.*, **83**, 3–15, https://doi.org/10.1016/S0034-4257(02)00084-6.

Koster, R. D., and Coauthors, 2004: Regions of strong coupling between soil moisture and precipitation. *Science*, **305**, 1138–1140, https://doi.org/10.1126/science.1100217.

Lawler, J. J., and Coauthors, 2014: Protected land-use change impacts on ecosystem services in the United States. *Proc. Natl. Acad. Sci. USA*, **111**, 7492–7497, https://doi.org/10.1073/pnas.1405557111.

Li, M., Y. Song, X. Huang, J. Li, Y. Mao, T. Zhu, X. Cai, and B. Liu, 2014: Improving mesoscale modeling using satellite-derived land surface parameters in the Pearl River Delta region, China. *J. Geophys. Res. Atmos.*, **119**, 6325–6346, https://doi.org/10.1002/2014JD021871.

Loveland, T. R., T. L. Sohl, S. V. Stehman, A. L. Gallant, K. L. Sayler, and D. E. Napton, 2002: A strategy for estimating the rates of recent United States land-cover changes. *Photogramm. Eng. Remote Sens.*, **68**, 1091–1099.

Mahmood, R., K. G. Hubbard, and C. Carlson, 2004: Modification of growing-season surface temperature records in the northern Great Plains due to land-use transformation: Verification of

modelling results and implication for global climate change. *Int. J. Climatol.*, **24**, 311–327, https://doi.org/10.1002/joc.992.
——, S. A. Foster, T. Keeling, K. G. Hubbard, C. Carlson, and R. Leeper, 2006: Impacts of irrigation on 20th century temperature in the northern Great Plains. *Global Planet. Change*, **54** (1–2), 1–18, https://doi.org/10.1016/j.gloplacha.2005.10.004.
——, R. Leeper, and A. I. Quintanar, 2011: Sensitivity of planetary boundary layer atmosphere to historical and future changes of land use/land cover, vegetation fraction, and soil moisture in western Kentucky, USA. *Global Planet. Change*, **78**, 36–53, https://doi.org/10.1016/j.gloplacha.2011.05.007.
——, T. Keeling, S. A. Foster, and K. G. Hubbard, 2013: Did irrigation impact 20th century air temperature in the High Plains aquifer region? *Appl. Geogr.*, **38**, 11–21, https://doi.org/10.1016/j.apgeog.2012.11.002.
——, and Coauthors, 2014: Land cover changes and their biogeophysical effects on climate. *Int. J. Climatol.*, **34**, 929–953, https://doi.org/10.1002/joc.3736.
——, R. A. Pielke Sr., and C. A. McAlpine, 2016: Climate-relevant land use and land cover change policies. *Bull. Amer. Meteor. Soc.*, **97**, 195–202, https://doi.org/10.1175/BAMS-D-14-00221.1.
Mesinger, F., and Coauthors, 2006: North American Regional Reanalysis. *Bull. Amer. Meteor. Soc.*, **87**, 343–360, https://doi.org/10.1175/BAMS-87-3-343.
Nair, U. S., Y. Wu, J. Kala, T. J. Lyons, R. A. Pielke Sr., and J. M. Hacker, 2011: The role of land use change on the development and evolution of the west coast trough, convective clouds, and precipitation in southwest Australia. *J. Geophys. Res.*, **116**, D07103, https://doi.org/10.1029/2010JD014950.
Nakićenović, N., and Coauthors, 2000: *Special Report on Emissions Scenarios*. Cambridge University Press, 608 pp.
Nikolic, J., S. Zhong, L. Pei, X. Bian, W. E. Heilman, and J. J. Charney, 2019: Sensitivity of low-level jets to land-use and land-cover change over the continental U.S. *Atmosphere*, **10**, 174, https://doi.org/10.3390/atmos10040174.
Niu, G.-Y., and Coauthors, 2011: The community Noah land surface model with multiparameterization options (Noah–MP): 1. Model description and evaluation with local–scale measurements. *J. Geophys. Res.*, **116**, D12109, https://doi.org/10.1029/2010JD015139.
Pei, L., N. Moore, S. Zhong, A. D. Kendall, Z. Gao, and D. W. Hyndman, 2016: Effects of irrigation on summer precipitation over the United States. *J. Climate*, **29**, 3541–3558, https://doi.org/10.1175/JCLI-D-15-0337.1.
Pielke, R. A., Sr., 2005: Land use and climate change. *Science*, **310**, 1625–1626, https://doi.org/10.1126/science.1120529.
——, and Coauthors, 2011: Land use/land cover changes and climate: Modeling analysis and observational evidence. *Wiley Interdiscip. Rev.: Climate Change*, **2**, 828–850, https://doi.org/10.1002/wcc.144.
——, R. Mahmood, and C. McAlpine, 2016: Land's complex role in climate change. *Phys. Today*, **69**, 40–46, https://doi.org/10.1063/PT.3.3364.
Pitman, A. J., F. B. Avila, G. Abramowitz, Y. P. Wang, S. J. Phipps, and N. de Noblet-Ducoudré, 2011: Importance of background climate in determining impact of land-cover change on regional climate. *Nat. Climate Change*, **1**, 472–475, https://doi.org/10.1038/nclimate1294.
Pyke, C. R., and S. J. Andelman, 2007: Land use and land cover tools for climate adaptation. *Climatic Change*, **80**, 239–251, https://doi.org/10.1007/s10584-006-9110-x.
Segal, M., and R. W. Arritt, 1992: Non-classical mesoscale circulations caused by surface sensible heat-flux gradients. *Bull. Amer. Meteor. Soc.*, **73**, 1593–1604, https://doi.org/10.1175/1520-0477(1992)073<1593:NMCCBS>2.0.CO;2.
Skamarock, W. C., and Coauthors, 2019: A description of the Advanced Research WRF Model version 4. NCAR Tech. Note NCAR/TN-556+STR, 145 pp., https://doi.org/10.5065/1dfh-6p97.
Sleeter, B. M., T. Loveland, G. Domke, N. Herold, J. Wickham, and N. Wood, 2018: Land cover and land-use change. *Impacts, Risks, and Adaptation in the United States: Fourth National Climate Assessment*, Vol. II, D. R. Reidmiller et al., Eds., U.S. Global Change Research Program, 202–231, https://doi.org/10.7930/NCA4.2018.CH5.
Sohl, T. L., K. L. Sayler, M. A. Drummond, and T. R. Loveland, 2007: The FORE-SCE model: A practical approach for projecting land cover change using scenario-based modeling. *J. Land Use Sci.*, **2**, 103–126, https://doi.org/10.1080/17474230701218202.
——, and Coauthors, 2012: Spatially explicit land-use and land-cover scenarios for the Great Plains of the United States. *Agric. Ecosyst. Environ.*, **153**, 1–15, https://doi.org/10.1016/j.agee.2012.02.019.
——, and Coauthors, 2014: Spatially explicit modeling of 1992–2100 land cover and forest stand age for the conterminous United States. *Ecol. Appl.*, **24**, 1015–1036, https://doi.org/10.1890/13-1245.1.
——, M. C. Wimberely, V. C. Radeloff, D. M. Theobald, and B. M. Sleeter, 2016: Divergent projections of future land use in the United States arising from different models and scenarios. *Ecol. Modell.*, **337**, 281–297, https://doi.org/10.1016/j.ecolmodel.2016.07.016.
——, and Coauthors, 2018: Conterminous United States Land Cover Projections—1992 to 2100. U.S. Geological Survey, accessed 13 March 2019, https://doi.org/10.5066/P95AK9HP.
Spera, S. A., J. M. Winter, and J. W. Chipman, 2018: Evaluation of agricultural land cover representations on regional climate model simulations in the Brazilian Cerrado. *J. Geophys. Res. Atmos.*, **123**, 5163–5176, https://doi.org/10.1029/2017JD027989.
Torbick, N., D. Lusch, J. Qi, N. Moore, J. Olson, and J. Ge, 2006: Developing land use/land cover parameterization for climate–land modeling in East Africa. *Int. J. Remote Sens.*, **27**, 4227–4244, https://doi.org/10.1080/01431160600702426.
Veldkamp, A., and E. F. Lambin, 2001: Predicting land use change. *Agric. Ecosyst. Environ.*, **85** (1–3), 1–6, https://doi.org/10.1016/S0167-8809(01)00199-2.
Vogelmann, J. E., S. M. Howard, L. Yang, C. R. Larson, B. K. Wylie, and N. Van Driel, 2001: Completion of the 1990s National Land Cover Data Set for the conterminous United States from LandSat thematic mapper data and ancillary data sources. *Photogramm. Eng. Remote Sens.*, **67**, 650–662.
Wang, H. J., W. L. Shi, and X. H. Chen, 2006: The statistical significance test of regional climate change caused by land use and land cover variation in West China. *Adv. Atmos. Sci.*, **23**, 355–364, https://doi.org/10.1007/s00376-006-0355-0.
Wear, D. N., 2011: Forecasts of county-level land uses under three future scenarios: A technical document supporting the forest service 2010 RPA Assessment. USDA Forest Service Southern Research Station General Tech. Rep. SRS-141, 41 pp.
Wisse, J. S. P., and J. Vilà-Guerau de Arellano, 2004: Analysis of the role of the planetary boundary layer schemes during a severe convective storm. *Ann. Geophys.*, **22**, 1861–1874, https://doi.org/10.5194/angeo-22-1861-2004.
Zaitchik, B. F., J. A. Santanello, S. V. Kumar, and C. D. Peters-Lidard, 2013: Representation of soil moisture feedbacks during drought in NASA Unified WRF (NU-WRF). *J. Hydrometeor.*, **14**, 360–367, https://doi.org/10.1175/JHM-D-12-069.1.
Zhao, M., and A. J. Pitman, 2002: The regional scale impact of land cover change simulated with a climate model. *Int. J. Climatol.*, **22**, 271–290, https://doi.org/10.1002/joc.727.
——, ——, and T. Chase, 2001: The impact of land cover change on the atmospheric circulation. *Climate Dyn.*, **17**, 467–477, https://doi.org/10.1007/PL00013740.